Effective mass effect in attosecond electron transport

Kasmi, Lamia ; Lucchini, Matteo ; Castiglioni, Luca ; Kliuiev, Pavel ; Osterwalder, Jürg ; Hengsberger, Matthias ; Gallmann, Lukas ; Krüger, Peter ; Keller, Ursula

Abstract: The electronic band structure governs the electron dynamics in solids. It defines a group velocity and an effective mass of the electronic wave packet. Recent experimental and theoretical studies suggest that an electron acquires the effective mass of its excited state over distances much larger than the lattice period of the solid. Therefore, electron propagation on atomic length scales was typically considered to be free-electron-like. Here, we test this hypothesis by probing attosecond photoemission from a Cu(111) surface. We use attosecond pulse trains in the extreme-ultraviolet (21–33 eV) to excite electrons from two initial bands within the 3d-valence band of copper. We timed their arrival at the crystal surface with a probing femtosecond infrared pulse, and found an upper limit of 350±40 as (1 as=10−18 s) for the propagation time an electron requires to assume the effective mass of its excited state. This observation implies that a final-state Bloch wave packet forms within a travel distance of 5–7 Å, which is at most two atomic layers. Using well-established theory, our measurements demonstrate the importance of the band structure even for atomic-scale electron transport.

DOI: https://doi.org/10.1364/OPTICA.4.001492

optica

Effective mass effect in attosecond electron transport

Lamia Kasmi,[1,*] Matteo Lucchini,[1] Luca Castiglioni,[2] Pavel Kliuiev,[2] Jürg Osterwalder,[2] Matthias Hengsberger,[2] Lukas Gallmann,[1,3] Peter Krüger,[4] and Ursula Keller[1]

[1]Department of Physics, ETH Zurich, 8093 Zürich, Switzerland
[2]Department of Physics, University of Zurich, 8057 Zürich, Switzerland
[3]Institute of Applied Physics, University of Bern, 3012 Bern, Switzerland
[4]Graduate School of Science and Engineering, Chiba University, Chiba 263-8522, Japan
*Corresponding author: kasmil@phys.ethz.ch

Received 7 August 2017; revised 3 November 2017; accepted 6 November 2017 (Doc. ID 304021); published 30 November 2017

The electronic band structure governs the electron dynamics in solids. It defines a group velocity and an effective mass of the electronic wave packet. Recent experimental and theoretical studies suggest that an electron acquires the effective mass of its excited state over distances much larger than the lattice period of the solid. Therefore, electron propagation on atomic length scales was typically considered to be free-electron-like. Here, we test this hypothesis by probing attosecond photoemission from a Cu(111) surface. We use attosecond pulse trains in the extreme-ultraviolet (21–33 eV) to excite electrons from two initial bands within the 3*d*-valence band of copper. We timed their arrival at the crystal surface with a probing femtosecond infrared pulse, and found an upper limit of 350 ± 40 as (1 as = 10^{-18} s) for the propagation time an electron requires to assume the effective mass of its excited state. This observation implies that a final-state Bloch wave packet forms within a travel distance of 5–7 Å, which is at most two atomic layers. Using well-established theory, our measurements demonstrate the importance of the band structure even for atomic-scale electron transport.

OCIS codes: (260.7120) Ultrafast phenomena; (320.7130) Ultrafast processes in condensed matter, including semiconductors; (240.6675) Surface photoemission and photoelectron spectroscopy.

https://doi.org/10.1364/OPTICA.4.001492

1. INTRODUCTION

Electron mobility in semiconductor materials used, for example, in field-effect-transistors is a key parameter for the engineering of high-performance electronic devices [1]. The mobility directly depends on the effective mass of the electron in the crystal lattice. Reduced-structure sizes in integrated circuits and recent innovations towards atomic-scale transistors [1,2] lead to electron transport happening over distances of a few Ångströms that electrons traverse on attosecond time scales. Given that the idea of an effective electron mass originates from the assumption of an unbounded periodic crystal [3], the question arises whether it is still a valid concept on atomic-length and sub-femtosecond timescales [4].

Studies on ultracold atoms in optical lattices show that under the application of a sudden force, the effective mass needs time to get established [5,6]. Ultracold atoms in optical lattices to a certain extent mimic coherent quantum behavior occurring in solid-state systems [7]. This result challenges the widespread assumption that the electrons always "feel" their crystal surrounding, which predicts a dynamical behavior of the effective mass related to the transient response of the particle after perturbation [5]. Observing these dynamics in solid-state systems on attosecond timescales is not only relevant for atomic-scale circuitry, but also in understanding the process of high-harmonic generation in solids [5,8].

Attosecond photoemission experiments allow us to probe effective mass dynamics by triggering an electron transition using short attosecond light bursts in the extreme ultraviolet (XUV), which consists of a sudden perturbation to the unperturbed electronic system. The consecutive processes to the creation of the electron-hole pair range from screening of the hole by the remaining electrons and rearrangement of electron energetics through electron–electron correlation. These processes contribute to altering the potential environment that the newly excited electron experiences and might delay the change of its effective mass to that of its excited state. By measuring the escape velocity of the excited electron for short propagation distances, one can infer the dynamical characteristics of its transport and conclude on the final established effective mass.

Attosecond metrology has provided the first results with this kind of electron transport in solids looking at the escape time of photoemitted electrons [9–13] and considering a simple ballistic transport model. The question about the correct escape velocity of the electrons and whether their dynamics are controlled by the periodic crystal potential on such small time and length scales

has been debated [11,14,15–17], and mainly free-electron-like propagation was observed or deduced. Kinetic-energy-resolved measurements of the time delay from valence-band excitation, with reference to a gas target [18], led to observed delays that could not be fully explained by the free-electron escape velocity. However, a conclusive proof that the effective mass has become relevant in the electron transport could not be provided. In a more recent study, bulk final-state effects on photoemission delays were investigated with the conclusion that the effective mass does not have an effect on the electron escape time even when a resonant transition to a crystal Bloch wave takes place [17]. This result is surprising and counterintuitive, as this type of final state only appears through the interaction with the periodic crystal potential, which then also defines the electron group velocity and effective mass.

In this work, we observe a non-monotonic behavior of the photoemission delays as a function of electron kinetic energy, which hints at effects from bulk resonances. We attempt to address the role of the band structure in defining the escape velocity of an electron propagating on atomic length scales and attosecond timescales.

2. ABSOLUTE TWO-PHOTON, TWO-COLOR PHOTOEMISSION DELAY MEASUREMENT

A. Experiment

We are able to extract the *absolute* two-photon, two-color photoemission delays specific to the solid target by calibrating the data against an independent atomic gas-phase reference in a two-foci experimental arrangement [10,18–20] [see Fig. 1(a)].

We studied the energy-dependent electron escape time from a Cu(111) surface using an implementation of time- and angle-resolved photoemission spectroscopy (tr-ARPES) with attosecond resolution [10,18,19] [Fig. 1(a)]. The photoemission process is started by pulses in the XUV and probed by an infrared (IR) pulse [Fig. 1(b)] at the surface. Previously, we have experimentally confirmed the efficient screening of copper, which means that the probing IR field does not affect the electron transport to the surface [19]. This disentangles the effects of the probing and exciting fields and ensures that the extracted photoemission delays correspond to the average propagation time for the electrons to reach the surface [21]. This electron escape time can be described with the three-step model of photoemission [22], as schematically illustrated in Figs. 1(b) and 1(c).

We orient our Cu(111) sample to a region of the momentum space where the 3*d*-valence band is split into two separate bands [red dashed line in Figs. 2(b) and 2(c)]. At this angular position, the effect of the initial and final states can be addressed at the same time. Moreover, the degree of localization of the initial state is comparable for all the investigated *d*-bands and can thus be ruled out as the main source for delay variation in our experiment. For simplicity, we name the split parts of the 3*d*-valence band "lower" and "upper" [Figs. 2(b), 2(d), and 2(f)] based on their binding energy.

Figure 2(b) shows the electron yield as a function of kinetic energy and azimuthal angle for a given polar emission angle of 30° and photon incidence angle of 75°. In a scheme similar to the one used in Refs. [10,19], we gain access to the photoemission delays using the technique of reconstruction of attosecond beating by two-photon transitions (RABBITT) [24,25]. The RABBITT technique uses short bursts of XUV attosecond pulses formed by odd-order harmonics of the photon energy of an IR probe pulse [Fig. 2(a)]. The photoemission delays are encoded in the phase of oscillatory signals that are observed as a function of delay between the exciting XUV pulses and the probing IR field [Figs. 2(d) and 2(g)]. These signals are a consequence of quantum-path interference in a two-color, two-photon absorption process and appear as sidebands in the photoelectron spectrum, located between peaks produced through single-photon absorption of the attosecond-pulse-forming harmonics. The sidebands are thus labeled as even-order multiples of the IR photon energy. An argon gas target in a first focus of the experimental setup serves as a robust reference for the photoemission delay extraction [Fig. 2(e)]. Timing in the photoemission process is then extracted from the phase difference between sideband signals of the same order from the argon and solid surface targets, respectively [Figs. 2(f) and 2(g)]. This allows us to cancel out the effect of the attochirp associated with the XUV attosecond pulse train. By subtracting the theoretical values of the argon atomic delay [26], propagation delay [20], and the delay induced

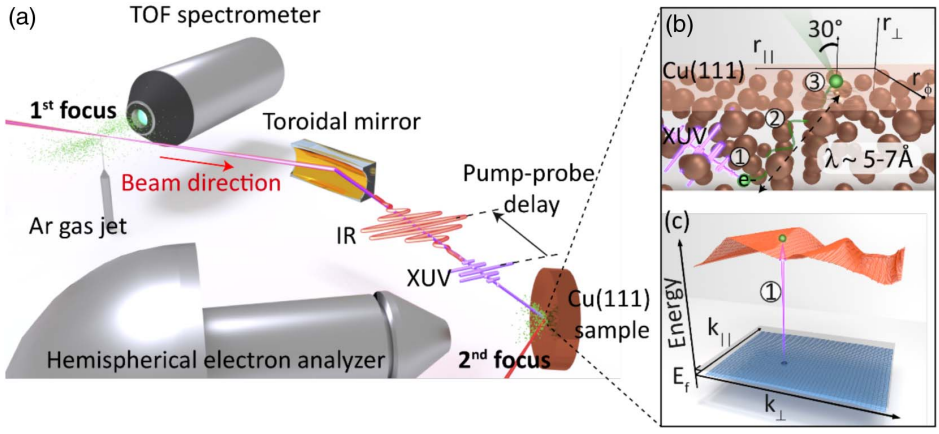

Fig. 1. (a) Experimental setup. The p-polarized XUV and IR beams are focused first into an argon gas target to obtain a reference RABBITT measurement. Subsequently, the pulses are refocused by a gold-coated toroidal mirror onto the copper sample at an incidence angle of 75°, and the photoelectrons are detected by a hemispherical analyzer 30° from the surface normal. A second RABBITT from copper is recorded. (b), (c), Sketch of the three-step model of photoemission. (1) Upon excitation by light, an electron is promoted from an occupied band in the valence band below the Fermi level into an unoccupied band. (2) The excited electron propagates in real space towards the solid surface. (3) The electron passes the surface barrier potential and escapes the solid, where it will then interact with the IR. With the given XUV photon energies, the typical photoelectron escape depths λ range between 5 and 7 Å.

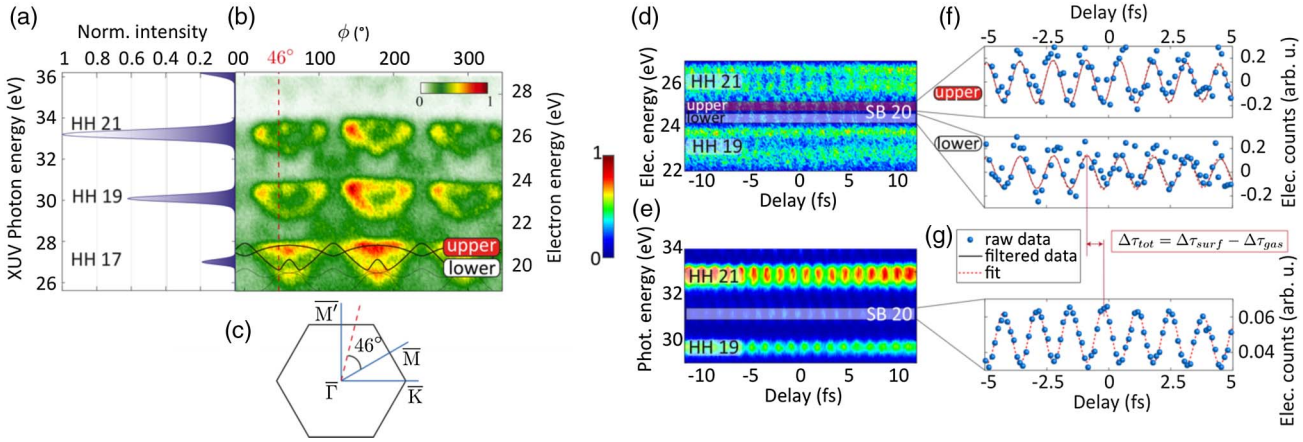

Fig. 2. Extraction of attosecond photoemission delays from split 3*d*-valence band. (a) XUV photon spectrum used in our experiment. (b) Each XUV harmonic ionizes the 3*d*-valence band of copper and gives a photoelectron signal from which the band structure can be retrieved [23]. The photoemission spectra are obtained at a detection angle of 30° from the surface normal and by rotating the copper sample around the (111) direction, hence varying the azimuthal angle ϕ. In black, the 3*d*-band structure of copper calculated with DFT is superimposed over the data measured with harmonic order 17. Thick lines highlight the two bands yielding high photoemission intensity; they are labeled with "upper" and "lower" according to their binding energy. (c) Sketch of the surface Brillouin zone with main crystallographic directions. The red dashed lines in (b) and (c), corresponding to $\phi = 46°$, indicate the position at which the RABBITT measurements were taken. $\phi = 0°$ corresponds to the $\overline{\Gamma M}$ direction. (d), (e) Portions of RABBITT traces measured from the copper sample at the second focus and from argon gas at the first focus, respectively. (f) Sideband 20, integrated over the respective split peaks and separated into an upper and lower part corresponding to the bands highlighted in (b). (g) Integrated sideband 20 in the argon RABBITT data that serves as the reference in the photoemission delay measurement.

by the IR transient grating forming at the surface of the solid target [19], we are able to extract the copper-surface-specific absolute two-photon, two-color photoemission delay. We refer the reader to Supplement 1 for more details on the measurement technique and delay extraction.

B. Results

The resulting photoemission delays for the two split parts of the 3*d*-valence band of copper are reported in Fig. 3. They show large

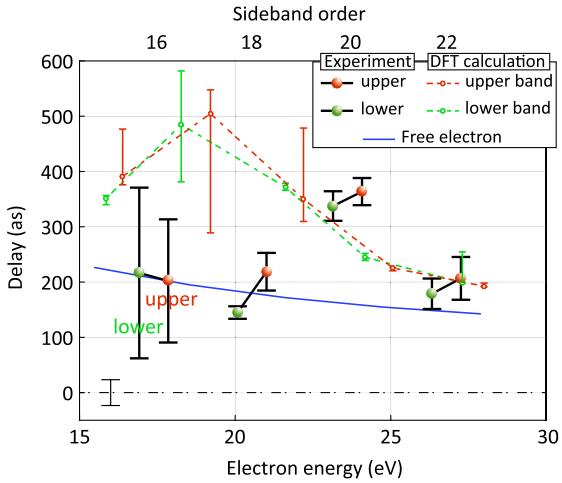

Fig. 3. Experimental results for photoemission delays (black) are plotted for upper and lower parts of the 3*d*-valence band as a function of the electron kinetic energy. The free-electron propagation time associated with mechanism (i) is plotted in blue. The propagation delays, based on group velocity derivation from the electronic band structure obtained from DFT calculations and associated with mechanism (ii), are plotted for the lower and upper parts of the 3*d*-valence band (in green and orange, respectively). The error bar around the zero level shows the uncertainty of our delay calibration.

variations on the order of a few hundreds of attoseconds and a non-monotonic trend with energy, suggesting delay contributions beyond free-electron transport period in particular in the energy region around 24 eV, the data points clearly deviate from the trend suggested by the remaining data and the measured photoemission delay amounts to 350 ± 40 as. In addition, the data also show an influence of the initial state with delays between the two initial bands ranging from 15 to 75 as, depending on the electron energy. The error bars in the experiment are the fit-related standard deviations for the retrieved delay across the different data sets (see Supplement 1).

In the process of RABBITT, the IR photon couples electrons ionized from two neighboring harmonics to interfere into the sideband signal of the RABBITT trace [27]. Provided that the target photoemission phase varies slowly with energy, RABBITT is very accurate in measuring the energy-dependent photoemission delays. The absolute two-photon, two-color photoemission delay extracted from our data τ_{2q}^{Cu} can be broken down into three terms [10]:

$$\tau_{2q}^{\mathrm{Cu}} = \tau_W + \tau_{\mathrm{transp}} + \tau_{cc}, \tag{1}$$

where $2q$ is the sideband order, τ_W is the Wigner delay due to the absorption of one XUV photon, τ_{transp} is the delay associated with the electron transport through the solid, and τ_{cc} is the measurement-induced delay due to the interaction with the IR probe field. $\tau_W + \tau_{cc}$ are on the order of tens of attoseconds. The transport delay is the dominant contribution to the total photoemission delay from a solid target in a regime where the photoelectrons travel more than ∼1 atomic monolayer [10].

Based on this, we assume τ_{2q}^{Cu} to be exclusively due to transport. Neglecting the $\tau_W + \tau_{cc}$ contribution results in an error of tens of attoseconds, which is acceptable given the error bars of our measurement. We thus compare the experimental τ_{2q}^{Cu} with the calculated transport times.

3. TRANSPORT DELAY CALCULATIONS WITHIN THE BALLISTIC TRANSPORT MODEL

It has been shown that photoemission delays measured with either the streaking or RABBITT technique are consistent with the average propagation time needed for an electron to reach the surface, provided that the IR skin depth is vanishing [21]. We verified that in case of copper, the internal IR field has a very low effect on the photoemission delays and therefore that this assumption is valid [19]. Therefore, we compare our experimental results with a ballistic transport model. This model relates the average propagation time measured through the photoemission delays to an average propagation distance, which here is the inelastic mean free path [28] and an average escape velocity. We distinguish two cases: (i) transitions to a free-electron-like final state, and (ii) transitions into a bulk final state described by a Bloch wave.

A. Free Electron Final-State Approximation

In order to determine the photoelectron momentum inside the solid, a common approximation is to assume that the dispersion relation inside the solid follows that of a free electron. This is the so-called *free-electron approximation* [23]

$$E_{\mathrm{kin,s}} = \frac{\hbar^2 k^2}{2m_e} - E_0, \tag{2}$$

where $E_{\mathrm{kin,s}}$ is the kinetic energy inside the solid, k is the electron momentum inside the solid, m_e is the electron bare mass, and E_0 is the inner potential value, which is 7.5 eV in the case of Cu(111) [29]. It follows that for a free-electron-like final state, the group velocity is given by

$$\vec{v}_{\mathrm{fe}}(\vec{k}) = \frac{\hbar\vec{k}}{m_e}. \tag{3}$$

Considering the energy-dependent inelastic mean free path, λ [28], we can derive the average propagation time within a simple ballistic transport model as

$$\tau_{\mathrm{fe}}(E_{\mathrm{kin}}) = \frac{\lambda(E_{\mathrm{kin}})}{|\vec{v}_{\mathrm{fe}}|} \tag{4}$$

(blue curve in Fig. 3), with E_{kin} being the photoelectron kinetic energy.

B. Bulk Final State

In the case of a resonant transition to a bulk final state, we took into account the actual band dispersion which defines the three-dimensional group velocity of the electron wave packet:

$$\vec{v}_g(\vec{k}) = \frac{1}{\hbar}\vec{\nabla}E(\vec{k}). \tag{5}$$

We performed density functional theory (DFT) calculations in the local density approximation to investigate the section of reciprocal space probed by our XUV pulse, in order to assess the role of the band structure in the measured delays. The calculated band structure is reported in Fig. 4(a) together with a cartoon of the two competing mechanisms following XUV excitation. We identified the momentum coordinates $(k_\parallel, k_\perp)$ of the excited electrons within the first Brillouin zone. The $k_\parallel$ coordinate is extracted from the ARPES measurement (see Supplement 1). We then calculated the escape time for a particular allowed transition at a fixed XUV photon energy and parallel momentum $k_\parallel$:

$$\tau_i(E_{\mathrm{kin}}) = \frac{\lambda(E_{\mathrm{kin}})}{|\vec{v}_g(k_\parallel, k_\perp^{(i)})|}. \tag{6}$$

The total transport time, still within the ballistic transport model, is calculated at the average kinetic energy $E_{\mathrm{kin,avg}}$ for a given XUV photon energy. It is given by the weighted sum of the contributions from all the possible transitions that are compatible with the given detection geometry and photon energies, considering again the inelastic mean free path λ [28]:

$$\tau(E_{\mathrm{kin,avg}}) = \frac{\sum_i w_i \tau_i(E_{\mathrm{kin}})}{\sum_i w_i}. \tag{7}$$

The weights in this averaging procedure correspond to the calculated photoemission probability for each transition as well as the XUV spectral power density at the particular photon energy.

We calculate the photoemission probability in the framework of the three-step model of photoemission [22], where the photoelectron emission process is broken up into the following three steps:

1. Photoexcitation of an electron inside the solid;
2. Transport to the surface;
3. Crossing of the surface potential barrier and escape into the vacuum.

The first step contains the band structure information; it consists of an optical transition from an occupied to an unoccupied bulk band. Since the momentum of the XUV photons is negligible compared to the Brillouin zone dimension, optical transitions in the bulk are direct and the crystal momentum vector is conserved. Here we follow the theory of Spanjaard *et al.* [30], who derived an expression of the photoelectron yield in the three-step model framework and showed its agreement with the one-step model. The photoemission intensity for given photon energy $\hbar\omega$, kinetic photoelectron energy E, and emission angle can be written as

$$\begin{aligned} N(E,\hbar\omega) \propto \frac{1}{\omega^2}\sum_{i,f} & T_f \times k_f \times \Theta(v_{g,f,\perp}) \times \frac{v_{g,f,\perp}}{v_{g,i,\perp}} \times |M^B_{i,f}|^2 \\ & \times \delta(\vec{k}_i - \vec{k}_f) \times \delta(p_\parallel/\hbar - k_{f,\parallel} + G_\parallel) \times \delta(E_f - E_i - \hbar\omega) \\ & \times \delta(E - E_f - W_f). \end{aligned} \tag{8}$$

Here, the sums run over occupied initial i and unoccupied final f bulk states, whose energies $E_{i,f}$ and crystal momenta $\vec{k}_{i,f}$ are restricted by the delta functions. T_f is the probability that an electron in state f is transmitted through the surface barrier. $v_{g,i,f,\perp}$ is the perpendicular (i.e., surface normal) component of the group velocity in the initial/final state. The term $\Theta(v_{g,f,\perp})$ reflects the fact that only electrons with outgoing group velocity are transported to the surface and contribute to the photocurrent. M^B_{fi} is the electric dipole transition matrix element. The parallel component of photoelectron momentum in vacuum, $p_\parallel$, is determined by the emission angles as detailed subsequently. $G_\parallel$ is a surface reciprocal lattice vector. W_f is the sample work function which, in the case of Cu(111), is 4.94 eV.

All quantities in Eq. (8) are extracted from DFT calculations except T_f, which we take as constant. This is justified by the fact that the transmission probability quickly approaches 1 for kinetic energies larger than the surface potential barrier V_0 (e.g., $T_f = 0.97$ for $E_{\mathrm{kin}} = V_0 \approx 15$ eV and a rectangular barrier).

We checked our photoemission theory against experimental data from Ilver and Nilsson [31] (see Supplement 1 for more details). To compute the photoemission signal, we extract all the resonant transitions along the perpendicular momentum direction for a parallel component of the crystal momentum defined by

$$k_{\parallel} = \frac{p_{\parallel}}{\hbar} + G_{\parallel}, \qquad p_{\parallel} = \sqrt{2m_e E_{\mathrm{kin},v}} \sin\theta, \tag{9}$$

where m_e is the electron mass and $E_{\mathrm{kin},v}$ is the kinetic energy in vacuum. $G_{\parallel}$ is chosen such that $k_{\parallel}$ lies in the first Brillouin zone. We used the following relation to determine the kinetic energy from the binding energy plot:

$$E_{\mathrm{kin},v} = \hbar\omega - E_b - W_f, \tag{10}$$

where E_b is the binding energy. Among all resonant bulk transitions, only those with final state waves propagating towards the surface ($v_{g,f,\perp} > 0$) contribute to the photocurrent. Therefore, we discard the transitions with $v_{g,f,\perp} < 0$.

4. DISCUSSION

The final delays calculated for resonant bulk transitions are displayed in Fig. 3 and compared with the experimental results. The error bars are defined by the standard deviations over all the possible resonant transitions for a given $k_{\parallel}$ (see Supplement 1 for more details).

Measuring the escape time of the photoelectron within the inelastic mean free path distance gives insights on the escape velocity of the electron and therefore indicates whether or not the band structure influences the electron dynamics. Here we observe that, depending on the excitation photon energy, the measured escape times agree (within error bars) with either the free-electron-like or band-structure model for the final state. Therefore, for the case of the escape velocity of the electron being dictated by the crystal band structure, the final state dynamics must be described by the effective mass of the electron. We collect electrons that are escaping within the inelastic mean free path distance of 5–7 Å from the surface and where the electron wave function in the solid is matched to a free-electron wave function in vacuum. Although the photoemitted electron can travel at the free electron velocity, our result shows that kinematics dictated by the bulk are not excluded even if the electron starts so close to the surface.

A recent study [12] could disentangle electron–electron scattering from screening effects in photoemission delays from solid state targets. In particular, the delay contribution of the screening effect was found to be negligible for electrons with a final state energy higher than 20 eV. This is in agreement with a former study performed in our group [10], where photoemission delays calculated with either a fully screened photohole or a fully unscreened photohole differed by less than 10 as. This is again confirmed in our present study, as the measured photoemission delays are in very good agreement with the calculated ones. The calculations involve a transport model that considers electron scattering only through the inelastic mean free path concept.

Furthermore, with our method, one can infer the differences in the Wigner and continuum–continuum delays between two subbands with the same orbital angular momentum quantum number. This can be done by evaluating the differences in photoemission delays between electrons coming from the lower and upper parts of the 3*d*-valence band, and comparing them with differences in transport delay only [Fig. 4(b)]. With our present

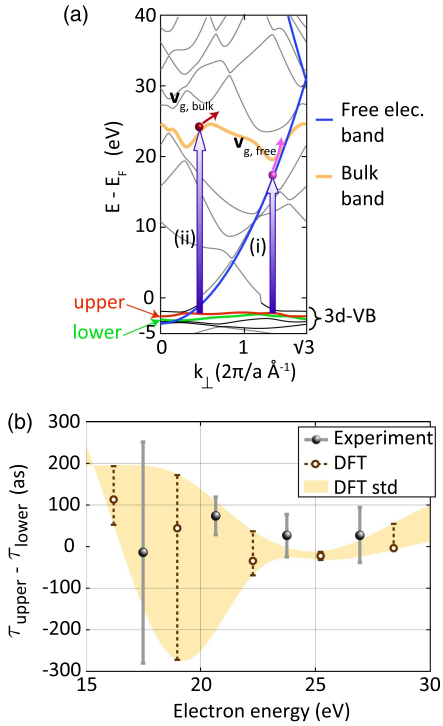

Fig. 4. (a) Scheme showing the two types of transitions that can occur: (i) transition into a free-electron final state and (ii) transition to a bulk final state. The different final band curvature for these two transitions determines the velocity at which the excited electron propagates towards the surface. (b) Difference between the experimental delays from the upper and lower parts of the 3*d*-valence band (in black), extracted from the experimental results shown in Fig. 3 together with the difference between the delays for transitions from the upper and lower parts of the valence band obtained with DFT calculations (in brown). The brown shaded area accounts for the standard deviation of the individual points.

data, the error bars are rather large, which makes it difficult to draw a conclusion. However, the observed trend may be seen as an indication of initial-state-dependent delays in the context of photoemission from solid-state targets. Initial-state-dependent delays have already been observed for states having different orbital angular-momentum quantum numbers. The measured delays were in the tens of attoseconds range [13]. The question as to whether initial states within the same electronic subshell undergo different photoemission delays—as would be the case in our experiment—has been investigated in the gas phase [32]; this investigation reported delay differences in Xe and Kr of about 30 and 8 as, respectively, originating from spin-orbit splitting. Conclusive evidence for a delay between electrons from the same subshell in a solid-state system will require further reduction of the error bars.

5. CONCLUSION

In this work, we were able to narrow down the precision of the escape velocity of electrons excited at different energies by extracting an absolute two-photon, two-color photoemission delay. We thereby show that, using an energy-dependent photoemission delay measurement, one can determine whether or not the electron dynamics can be affected by the crystal potential during the propagation. For the case in which the group velocity of

the band structure describes the escape velocity of the electron, we observe a significantly different photoemission delay, which implies that the effective mass must be established within the mean free path distance and within 350 ± 40 as. Our results demonstrate the need to consider the band structure in evaluating electron escape times at moderate electron energies of a few eV to tens of eV. Addressing the recent debate in this field, we have provided experimental evidence that the electron has time to "feel" the crystal potential and assume the effective mass of its final excited state even if the electron transport happens within 350 as and within a very short distance of 5–7 Å away from the surface. This result will be of major interest for understanding the scaling of electronic devices towards atomic dimensions, where transport times approach the attosecond regime and the theoretical assumptions of traditional solid-state physics concepts are challenged.

Funding. Schweizerischer Nationalfonds zur Förderung der Wissenschaftlichen Forschung (SNF) (NCCR MUST); Japan Society for the Promotion of Science (JSPS) (KAKENHI JP 16K05393).

See Supplement 1 for supporting content.

REFERENCES

1. M. Chhowalla, D. Jena, and H. Zhang, "Two-dimensional semiconductors for transistors," Nat. Rev. **1**, 1–15 (2016).
2. S. B. Desai, S. R. Madhvapathy, A. B. Sachid, J. P. Llinas, Q. Wang, G. H. Ahn, G. Pitner, M. J. Kim, J. Bokor, C. Hu, H. P. Wong, and A. Javey, "MoS2 transistors with 1-nanometer gate lengths," Science **354**, 99–102 (2016).
3. N. W. Ashcroft and N. D. Mermin, *Solid State Physics* (Holt, 1976).
4. M. Gertsvolf, M. Spanner, D. M. Rayner, and P. B. Corkum, "Demonstration of attosecond ionization dynamics inside transparent solids," J. Phys. B **43**, 131002 (2010).
5. R. Chang, S. Potnis, R. Ramos, C. Zhuang, M. Hallaji, A. Hayat, F. Duque-Gomez, J. E. Sipe, and A. M. Steinberg, "Observing the onset of effective mass," Phys. Rev. Lett. **112**, 170404 (2014).
6. F. Duque-Gomez and J. E. Sipe, "Response of a particle in a one-dimensional lattice to an applied force: dynamics of the effective mass," Phys. Rev. A **85**, 053412 (2012).
7. I. Bloch, J. Dalibard, and W. Zwerger, "Many-body physics with ultracold gases," Rev. Mod. Phys. **80**, 885–964 (2008).
8. S. Ghimire, A. D. DiChiara, E. Sistrunk, P. Agostini, L. F. DiMauro, and D. A. Reis, "Observation of high-order harmonic generation in a bulk crystal," Nat. Phys. **7**, 138–141 (2010).
9. A. L. Cavalieri, N. Muller, T. Uphues, V. S. Yakovlev, A. Baltuska, B. Horvath, B. Schmidt, L. Blumel, R. Holzwarth, S. Hendel, M. Drescher, U. Kleineberg, P. M. Echenique, R. Kienberger, F. Krausz, and U. Heinzmann, "Attosecond spectroscopy in condensed matter," Nature **449**, 1029–1032 (2007).
10. R. Locher, L. Castiglioni, M. Lucchini, M. Greif, L. Gallmann, J. Osterwalder, M. Hengsberger, and U. Keller, "Energy-dependent photoemission delays from noble metal surfaces by attosecond interferometry," Optica **2**, 405–410 (2015).
11. S. Neppl, R. Ernstorfer, A. L. Cavalieri, C. Lemell, G. Wachter, E. Magerl, E. M. Bothschafter, M. Jobst, M. Hofstetter, U. Kleineberg, J. V. Barth, D. Menzel, J. Burgdorfer, P. Feulner, F. Krausz, and R. Kienberger, "Direct observation of electron propagation and dielectric screening on the atomic length scale," Nature **517**, 342–346 (2015).
12. C. Chen, Z. Tao, A. Carr, P. Matyba, T. Szilvasi, S. Emmerich, M. Piecuch, M. Keller, D. Zusin, S. Eich, M. Rollinger, W. You, S. Mathias, U. Thumm, M. Mavrikakis, M. Aeschlimann, P. M. Oppeneer, H. Kapteyn, and M. Murnane, "Distinguishing attosecond electron-electron scattering and screening in transition metals," Proc. Natl. Acad. Sci. USA **114**, E5300–E5307 (2017).
13. F. Siek, S. Neb, P. Bartz, M. Hensen, C. Struber, S. Fiechter, M. Torrent-Sucarrat, V. M. Silkin, E. E. Krasovskii, N. M. Kabachnik, S. Fritzsche, R. D. Muino, P. M. Echenique, A. K. Kazansky, N. Muller, W. Pfeiffer, and U. Heinzmann, "Angular momentum-induced delays in solid-state photoemission enhanced by intra-atomic interactions," Science **357**, 1274–1277 (2017).
14. C. Lemell, B. Solleder, K. Tőkési, and J. Burgdörfer, "Simulation of attosecond streaking of electrons emitted from a tungsten surface," Phys. Rev. A **79**, 062901 (2009).
15. A. K. Kazansky and P. M. Echenique, "One-electron model for the electronic response of metal surfaces to subfemtosecond photoexcitation," Phys. Rev. Lett. **102**, 177401 (2009).
16. E. E. Krasovskii, "Attosecond spectroscopy of solids: streaking phase shift due to lattice scattering," Phys. Rev. B **84**, 195106 (2011).
17. Z. Tao, C. Chen, T. Szilvasi, M. Keller, M. Mavrikakis, H. Kapteyn, and M. Murnane, "Direct time-domain observation of attosecond final-state lifetimes in photoemission from solids," Science **353**, 62–67 (2016).
18. R. Locher, M. Lucchini, J. Herrmann, M. Sabbar, M. Weger, A. Ludwig, L. Castiglioni, M. Greif, M. Hengsberger, L. Gallmann, and U. Keller, "Versatile attosecond beamline in a two-foci configuration for simultaneous time-resolved measurements," Rev. Sci. Instrum. **85**, 013113 (2014).
19. M. Lucchini, L. Castiglioni, L. Kasmi, P. Kliuiev, A. Ludwig, M. Greif, J. Osterwalder, M. Hengsberger, L. Gallmann, and U. Keller, "Light-matter interaction at surfaces in the spatiotemporal limit of macroscopic models," Phys. Rev. Lett. **115**, 137401 (2015).
20. F. Schlaepfer, A. Ludwig, M. Lucchini, L. Kasmi, M. Volkov, L. Gallmann, and U. Keller, "Gouy phase shift for annular beam profiles in attosecond experiments," Opt. Express **25**, 3646–3655 (2017).
21. C. H. Zhang and U. Thumm, "Streaking and Wigner time delays in photoemission from atoms and surfaces," Phys. Rev. A **84**, 033401 (2011).
22. C. N. Berglund and W. E. Spicer, "Photoemission studies of copper and silver: theory," Phys. Rev. **136**, A1030–A1044 (1964).
23. A. Damascelli, "Probing the electronic structure of complex systems by ARPES," Phys. Scripta **T109**, 61–74 (2004).
24. H. G. Muller, "Reconstruction of attosecond harmonic beating by interference of two-photon transitions," Appl. Phys. B **74**, s17–s21 (2014).
25. P. M. Paul, E. S. Toma, P. Breger, G. Mullot, F. Auge, P. Balcou, H. G. Muller, and P. Agostini, "Observation of a train of attosecond pulses from high harmonic generation," Science **292**, 1689–1692 (2001).
26. A. S. Kheifets, "Time delay in valence-shell photoionization of noble-gas atoms," Phys. Rev. A **87**, 063404 (2013).
27. L. Cattaneo, J. Vos, M. Lucchini, L. Gallmann, C. Cirelli, and U. Keller, "Comparison of attosecond streaking and RABBITT," Opt. Express **24**, 29060–29076 (2016).
28. D. R. Penn, "Electron mean-free-path calculations using a model dielectric function," Phys. Rev. B **35**, 482–486 (1987).
29. S. Hüfner, *Photoelectron Spectroscopy: Principles and Applications* (Springer, 2003).
30. D. J. Spanjaard, D. W. Jepsen, and P. M. Marcus, "Effects of transmission factors and matrix elements on angular distribution of photoemission from Ag(111)," Phys. Rev. B **15**, 1728–1737 (1977).
31. L. Ilver and P. O. Nilsson, "Angular-resolved u.v. photoemission from single crystals of copper," Solid State Commun. **18**, 677–680 (1976).
32. I. Jordan, M. Huppert, S. Pabst, A. S. Kheifets, D. Baykusheva, and H. J. Wörner, "Spin-orbit delays in photoemission," Phys. Rev. A **95**, 013404 (2017).